Journal of Materials Chemistry C

Accepted Manuscript

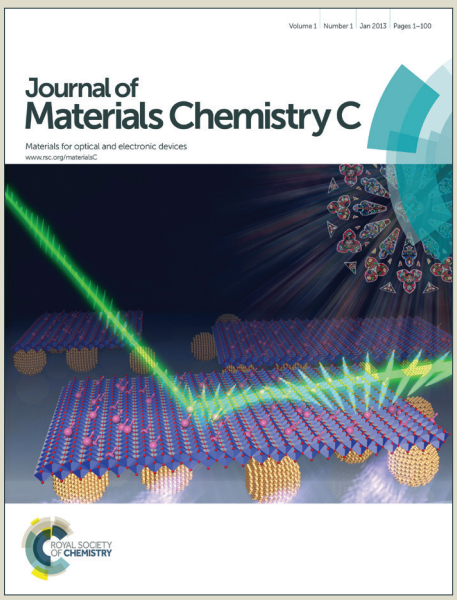

ROYAL SOCIETY OF CHEMISTRY

www.rsc.org/materialsC

Preparation and Characterization of Luminescent Silicone Elastomer by Thiol–ene "click" Chemistry

Yujing Zuo[a], Haifeng Lu[a], Lei Xue[a], Xianming Wang[b], Liang Ning[b], Shengyu Feng[a]*

a. Key Laboratory of Special Functional Aggregated Materials, Ministry of Education, School of Chemistry and Chemical Engineering, Shandong University, Jinan 250100, P. R. China

b. Marine Chemical Research Institute Company Limited and State Key Laboratory of Marine Coatings, Qingdao, P. R. China

Corresponding author: Shengyu Feng

Fax: +86–531–88564464;

Tel: +86–531–88364866;

E–mail: fsy@sdu.edu.cn

Abstract

Novel transparent and luminescent silicone elastomers were prepared by thiol–ene chemistry. They show very intense photoluminescence under ultraviolet light and have very high coloric purity. The luminescence was obtained by complexing lanthanide ions into a N–acetyl–L–cysteine functionalized polysiloxane. The functionalized polysiloxane was prepared by an easy thiol–ene reaction and the polysiloxane cured by thiol–ene reaction to get crosslinking network. Their structures and properties were characterized thoroughly. The experimental results indicate complexing lanthanide ions reduced the contact angles.

1. Introduction

The photoluminescence (PL) of trivalent lanthanide ions upon ultraviolet light irradiation is both scientifically and industrially relevant because the involvement of lanthanide ion compounds in efficient light–conversion molecular devices as phosphors in full–color, flat–panel displays, bio–probes, memory devices, and sensors [1, 2]. Lanthanide complexes have been researched thoroughly as practical luminescent materials because of their long–lived, excited–state characteristic and especially efficient, strong narrow–width, visible emission bands [3-5]. However, small lanthanide complexes are unstable without organic solutions and tend to dissociate into less–complex forms [6, 7]. The poor thermal stability and mechanical properties of lanthanide complexes also limit their application as luminophors [8].

Trapping lanthanide complexes in polymer backbone is a new method to generate luminescent materials and to overcome the limitations listed above. These materials have excellent properties, such as mechanical flexibility and convenient processability [9-13].

Lanthanide–doped polymer materials can be categorized into two main classes according to the chemical nature and synergy between components. The first class concerns systems in which only weak interactions between organic and inorganic parts are observed but no covalent bonds exist. The corresponding doping methods seem hard to prohibit the problem of the inhomogeneous dispersion of two phases, so the application of this sort of materials is largely restricted [14-16].

Therefore, another attractive possibility in regard to complexation of lanthanide ions using ligands that are covalently bonded to the polymer matrixes has emerged. For instance, Sun et al. have prepared a range of Eu^{3+} coordinated polymethyl methacrylates with good

luminescent properties. Combining functionalized polysiloxane and lanthanide complexes can construct useful materials that possess the outstanding properties of both. The organic groups in the functionalized polysiloxane can reinforce the energy absorbability in chromophoric groups, and the energy can be efficiently transferred to the lanthanide ions [17]. We have synthesized carbonyl functional polysiloxanes and incorporated them with lanthanide ions to obtain lanthanide–polysiloxane luminescent materials[18-21].

However, the mechanical properties of those lanthanide–coordinated polymers were poor because they were prepared in solution and the mechanical properties were destroyed when the solution was removed. Further work was developed to solve this problem. The lanthanide complex was synthesized firstly and then polymerized using the unsaturated bond in the ligand by Zhang et al [22]. The obtained materials showed good mechanical properties but the residual lanthanide complex cannot be efficiently eliminated.

In this paper, a novel synthetic method was suggested to obtain the luminescent silicone elastomers by complexing lanthanide ions into functionalized polysiloxane and then crosslinking by thiol–ene "click" reaction. In this method, the coordination process was done in solution to enhance the coordination efficiency between lanthanide ions and ligands and the cure process was done without solution to avoid the defect of solution mentioned above. Thiol–ene "click" reactions can withstand mild reaction conditions, can be generated with little solvent that can be easily removed, do not require expensive transition–metals as catalysts, and can react with little photoinitiator[23-29]. A variety of networks with a regular structure can be obtained using its unique step–growth mechanism, as shown in Scheme 1. Thiol–ene networks have a tremendous advantage over traditional ones because they can form

rapidly and quantitatively under ambient atmosphere [30].

Scheme 1

Luminescent silicone elastomer was prepared by facile thiol–ene reaction for the first time in this paper. A range of polysiloxanes containing cysteine groups were obtained by thiol–ene reaction and then coordinated with different lanthanide ions of Eu^{3+}, Tb^{3+} and Dy^{3+} to synthesize luminescent polysiloxanes. Luminescent polysiloxanes can be partially functionalized in the first step of the thiol−ene "click" process by controlling the molar ratio of vinyl–functioned polysiloxanes to N–Acetyl–L–cysteine (NAL) monomers. Residual vinyl group could be used as crosslinking sites. Then two–step sequential thiol−ene "click" reaction was applied to prepare polysiloxane–based elastomers. By using of 2,2'–1,2–ethanediylbis(oxy)bis(ethanethiol) (DBOET) and vinyl containing functional polysiloxane, it is possible to generate a crosslinked flexible stereoregular elastomer. This research was expected to offer a method to synthesize a lanthanide ion–containing silicone elastomer and this cure process could be used to prepare other kind of elastomer by easy thiol–ene "click" reaction.

Figure 1

2. Experimental

2.1 Materials

2,2–Dimethoxy–2–phenylacetophenone (DMPA) and N–Acetyl–L–cysteine (NAL) were purchased from Aladdin Co. (China) and used as received. Octamethylcyclotetrasiloxane (D_4), tetramethyltetravinylcyclotetrasiloxane (D_4^{Vi}), and hexamethyldisiloxane (MM) were obtained as commercial products and used directly. DBOET (95%) was provided by

Sigma–Aldrich and used as received. Tetrahydrofuran (THF) was purified according to routine procedure and distilled over sodium before use. Europium, terbium and dysprosium nitrates were obtained from their corresponding oxides in strong nitric acid.

2.2 Characterization and measurements

The reaction was irradiated by UV on a Spectroline Model SB–100P/FA lamp (365 nm, 100 w). UV intensity is 4500μW/cm ^{2} at a distance of 38 cm. Proton nuclear magnetic resonance (^{1}H NMR) spectra were recorded on a Bruker AVANCE 400 spectrometer at 25 °C using $CDCl_3$ as solvent and without tetramethylsilane as an interior label. Ultraviolet absorption (UV) spectra in THF solution were detected using a Beijing TU–1901 double beam UV–Vis spectrophotometer. Dynamic mechanic analysis (DMA) of the elastomer was conducted using a DMA analyzer in shear mode (METTLERDMASDTA861, USA). The specimens (5.00 mm × 4.60 mm × 1.68 mm) were analyzed at a frequency of 1 Hz with temperatures ranging from −100 °C to 0 °C given a heating rate of 3 °C/min in air atmosphere. Fourier transform infrared spectra (FT–IR) were recorded on a Bruker TENSOR27 infrared spectrophotometer using the KBr pellet technique within the 4000 cm^{-1} to 400 cm^{-1} region. Thermogravimetric analysis (TGA) was performed under N_2 using a TA SDTQ600 at a temperature range of room temperature to 800 °C with a heating rate of 10 °C/min. Contact angle was detected using a Data physics OCA–20 contact angle analyzer with distilled water as the test liquid. Scanning electronic microscopy (SEM) images were obtained using Hitachi S–4800 (7 kV). The samples were cut and coated with a thin layer of gold before the investigation. The luminescence (excitation and emission) spectra of the samples were determined with a Hitachi F–4500 fluorescence spectrophotometer using a monochromated

Xe lamp as an excitation source. Excitation and emission slits measured 5 nm and 2.5 nm, respectively. X–ray photoelectron spectroscopy was performed using a Thermo Fisher Scientific Escalab 250 spectrometer with a monochromated Al Ka X–ray source at a residual pressure of 10^{-7} Pa. The survey and high–resolution scans were generated at 100 eV pass energy with 1 eV step and 20 eV pass energy with 0.05 eV step, respectively.

2.3 Synthesis of Vinyl–functional Polysiloxanes (P1，P2)

Polymethylvinylsiloxane (**P1**)）was synthesized according to the classical procedure [31]. D_4 (20.0 g, 0.067 mol), D_4^{Vi} (20.0 g, 0.058 mol), and 0.20 g tetramethylammonium hydroxide were added to a three–neck flask with a stir bar and condenser under dry argon atmosphere. The mixture was stirred for 1 h at 100 °C to obtain a preformed polymer. MM (2.94 g, 17.6 mmol) was then added to the three–neck flask. The mixture was stirred for another 4 h at 100 °C and then heated to 140 °C to remove the tetramethylammonium hydroxide. P1 was obtained as a colorless liquid after low molecular–weight products were eliminated under vacuum at 180 °C. Yield: 90 %. ^{1}H NMR (400 MHz, $CDCl_3$, ppm): δ = 0.06 to 0.17 (m,–CH_3), δ = 5.79 to 6.03 (m, –CH = CH_2).

Vinyl–terminated polysiloxane (**P2)** was synthesized through the classical procedure [31]. D_4 (25.0 g, 0.085 mol), MM^{Vi} (0.97 g, 5.2 mmol), and 0.25 g tetramethylammonium hydroxide were added to a three–neck flask with a stir bar and condenser under dry argon atmosphere. The mixture was stirred for 4 h at 90 °C and then heated to 150 °C to eliminate tetramethylammonium hydroxide. P2 was obtained as a colorless liquid after low molecular–weight products were removed under vacuum at 180 °C. Yield: 92 %, ^{1}H NMR (400 MHz, $CDCl_3$, ppm): δ = 0.06 to 0.09 (m, –CH_3), 5.69 to 6.20 (m, –CH = CH_2).

2.4 Synthesis of NAL Functionalized polysiloxane (PNL and T–PNL) by thiol–ene reaction

The structure and synthetic route are shown in Scheme 2. NAL–functionalized polysiloxane (**PNL**) was synthesized by a literature procedure [31]. 1.62 g (10 mmol) N–acetyl–cysteine, 8.10 g (100 mmol) P1, and 0.08 g (0.3 mmol) DMPA were dissolved in glass vessels containing a mixed solvent of dry THF and CH_3OH with a volume ratio of 4:1. The vessels were placed under UV light irradiation(365 nm,100 w) and stirred gently for 10 min. The product was purified by methanol precipitation, followed by vacuum drying at room temperature for 24 h. Yield: 99%. ^{1}H NMR (400 MHz, $CDCl_3$, ppm): δ = 0.01 to 0.25 (m, –Si*CH*$_3$), 0.89 to 0.95 (m,–Si*CH*$_2$CH$_2$S–), 2.11 (s, –CO*CH*$_3$), 2.58 to 2.71 (m, –SiCH$_2$*CH*$_2$S–), 3.04 to 3.13 (m,–S*CH*$_2$CH–), 4.75 to 4.80 (m, –*CH*(COOH)–), 6.38 to 6.40 (d, –NHCO*CH*$_3$), 5.78 to 6.02 (m, –*CH*=*CH*$_2$).

Terminal NAL–functionalized polysiloxane (**T–PNL)** was obtained by a similar procedure. Yield: 99%. ^{1}H NMR (400 MHz, $CDCl_3$, ppm): δ = 0.01 to 0.25 (m, –Si*CH*$_3$), 0.89 to 0.95 (m,–Si*CH*$_2$CH$_2$S–), 2.11 (s, –CO*CH*$_3$), 2.58 to 2.71 (m, –SiCH$_2$*CH*$_2$S–), 3.04 to 3.13 (m,–SCH$_2$*CH*–), 4.75 to 4.80 (m, –*CH*(COOH)–), 6.38 to 6.40 (d, –NHCO*CH*$_3$). The gel permeation chromatography (GPC) data of P1, P2, PNL, and T–PNL are listed in Table 1.

Scheme 2

Table 1

2.5 Preparation of PNL–Lns and T–PNL–Lns by Lanthanide Metal Coordination

A series of complexes (Table 2) was prepared following the same procedure. PNL (2.54 g, 1.0 mmol) was dissolved in 15 ml THF with stirring, and $Eu(NO_3)_3{\cdot}6H_2O$（1.16 g, 2.61

mmol）was added to the solution. The mixture was refluxed for 4 h under magnetic stirring. The solvent was removed by vacuum to obtain a transparent viscous liquid (denoted as PNL–Eu1:1).

2.6 Preparation of silicone elastomers (PNL–Ln–SHs) by thiol–ene reaction

The preparation method is shown in Scheme 3. Crosslinking was achieved by a mixture of the PNL–Lns and bifunctional crosslinker DBOET at a molar ratio of 1:10 (thiol: vinyl functional groups). The lanthanide metal–coordinated PNL–Ln (5.33 g, 2.0 mmol) was dissolved in THF. DBOET (0.02 g, 0.1 mmol) and DMPA (0.001 g, 0.003 mmol) were gradually added to the mixtures. The mixture was poured into a Teflon mold and the solvent was evaporated. The mold was cured under UV lamp irradiation (365 nm, 100 w) to obtain a transparent silicone elastomer (**PNL–Ln–SHs**). Finally, the obtained elastomers were submerged in THF for 72 h. THF was changed every 24 h to ensure that all uncrosslinked material and photoinitiator residue could be removed from the network.

Scheme 3

Table 2

2.7 Measurement of crosslinking density

Silicone elastomer swelling degree was determined using a toluene swelling method reported in the literature [32, 33]. All of the experiments were performed in triplicate. The sample was dried in a vacuum oven for approximately 48 h before submergence and then immersed in toluene for approximately 48 h at room temperature. The solvent was changed every 12 h. The swollen gels were removed from the liquid, and excess solvent was wiped off the surface using filter paper. The gels were then carefully weighed. The equilibrium toluene content in

the sample was determined using Eq. (1):

$$\%swelling = (\frac{W_t - W_o}{W_o}) \times 100 \quad (1)$$

where W_0 is the weight of the dried polymer and W_t is the weight of the swollen polymer. φ can then be obtained by Eq. (2):

$$\varphi = \frac{W_o / \rho_2}{[(W_t - W_o)/\rho_1 + W_o/\rho_1]} \quad (2)$$

where ρ_1 and ρ_2 are the densities of the solvent and the polymer, respectively.

Molecular weights between the crosslinking points (Mc) were calculated using Flory and French's Eq. (3):

$$Mc = \frac{-\rho_2 V_0 \varphi^{1/3}}{[\ln(1-\varphi) + \varphi + \chi\varphi_2]} \quad (3)$$

where Mc is the average molecular weight between crosslink points, V_o is solvent volume, ρ_2 is the density of the silicone elastomer before use, and χ denotes the Flory–Huggins interaction parameter between polysiloxane and toluene (0.465).

Finally, crosslinking density (υ) could be obtained using Eq. (4):

$$\upsilon = \frac{\rho_1}{Mc} \quad (4)$$

3. Results and discussion

FT–IR spectra analysis

The FT–IR spectra for P1, NAL, PNL, and PNL–Eu are shown in Fig. 2 (a). The peak observed at 3054 cm^{-1} and 1598 cm^{-1} in curve of P1 are υ(C=C–H) and υ(C=C) vibrations respectively. The curve of NAL shows *st*(S–H) vibration at 2574 cm^{-1}. The υ(C=O) vibration is observed at 1734 cm^{-1} in the curve of PNL, which indicates the occurrence of the thiol–ene

reaction. The integral area of the peak at 3054 cm^{-1} and 1598 cm^{-1} diminished after thiol–ene reaction. This result also proved the success of NAL functionalization. The disappearance of *st*(S–H) vibration in the curve of PNL indicates that no residual NAL existed and the thiol–ene reaction was complete. A wide peak at 3341 cm^{-1} is generated by the combination of –OH stretch vibration in –COOH and –NH– stretch vibration in –CONH–. The shift of a peak from 3341 cm^{-1} to 3310 cm^{-1} and the increase in the integrate area in the curve PNL-Tb may be caused by small amounts of H_2O in the $Eu(NO_3)_3 \cdot 6H_2O$. Two sharp peaks observed at 1734 cm^{-1} and 1660 cm^{-1} can be attributed to the υ(C=O) vibration mode at –COOH and –OC–NH, respectively. The peak at 1660 cm^{-1} apparently shifts to 1626 cm^{-1}, as shown in curve PNL–Tb. The shift in υ(C=O) vibration to a lower wavenumber indicates the coordination between the C=O group and lanthanide ions [34]. There is a peak at 1734 cm^{-1} but the integral area of this peak decreased after coordination which means that the C=O group in –COOH partly coordinated with Ln^{3+}. This just because the hinder of the framework of polymer. We also synthesized T–PNL as a model compound to understand the coordination condition further. Related FT–IR spectra are shown in Fig. 2. (b). Peaks at 1734 cm^{-1} and 1660 cm^{-1} are observed. This result shows that the different positions of functional groups did not affect infrared absorption. Both the peak at 1734 cm^{-1} and the peak at 1660 cm^{-1} in T–PNL shifted to 1628 cm^{-1}. The apparent variation indicated the perfect coordination of lanthanide ions with both –COOH and –CONH–. This perfectly coordination exist justly when there is no hinder of the framework of polymer. This result confirmed our previous inference. Possible coordination structure of PNL–Lns was shown in Scheme 3. The Si–O–Si peak does not change; thus, the Si–O–Si bond did not act on Ln^{3+} in the process of

coordination.

Figure 2

Ultraviolet absorption spectra

The UV spectra of the PNL–Eu and T–PNL–Eu dispersed in THF were measured at room temperature at a concentration of 10^{-5} mol/L, as depicted in Fig. 3 (a). The PNL and PNL–Eu absorption spectra reveal that maximum absorption occurred at 240 nm with a shoulder at 276 nm, which are areas assigned to the $\pi \rightarrow \pi^*$ electronic transition of the carbonyl group and the $n \rightarrow \pi^*$ electronic transition, respectively [20, 35]. The change trend of T–PNL (Fig. 3 (b)) is similar to that of PNL. However, they varied significantly after coordination at 276 nm. PNL–Eu1:1 curve was generally consistent with those of PNL–Eu2:1. The increase in the Eu^{3+} molar ratio from 2:1 to 1:1 did not affect the absorption spectra which means that the absorbed energy in luminescence mainly come from the polymer matrix.

Figure 3

X–ray photoelectron spectroscopy analysis

XPS is an effective tool to characterize the coordination condition via detecting the binding energy between ligand and central ion. The coordination bonds of lanthanide ion complexes have polar covalent bond properties, as reported in previous research. Hence, the formation of coordination bonds is accompanied by electron transfer between ligands and the central ions. Coordination bonds have two forms, σ and back–donating π bonds; coordination complexes with carbonyl groups as ligands belong to the former. A single pair of electrons donated by ligands are transferred to the metallic ions as electron acceptors in σ–bond type

coordination complexes, and this process strengthens electron shielding and reduces the inner electron binding energy in metallic ions. The binding energy of the coordinated metallic ions decreases as the coordination ability of the ligands increases [36, 37]. The binding energy curves of Tb^{4d} of PNL–Tb2:1–SH and $Tb(NO_3)_3 \cdot 6H_2O$ are shown in Fig. 4. The peak of Tb 4d appears at 151.8 eV in terbium nitrate but the Tb 4d peaks shifted to higher binding energy at 153.6 eV (double–bond equivalent = 1.8 eV) in PNL–Tb2:1–SH. A conclusion could be drawn that all lanthanide ions coordinated with C=O groups in PNL–Tb2:1–SH [38].

Figure 4

Photoluminescence of the PNL–Lns and PNL-Ln-SHs

The emission spectrum of PNL–Lns2:1 in THF solution was shown in Figure 5. We excited solutions at 320 nm. PNL–Eu2:1 exhibits photoluminescence with a strong, sharp and well resolved emission at 617 nm that can be ascribed to the electric–dipole $^5D_0 \rightarrow {}^7F_2$transition of the Eu^{3+} ions. A minor emission peak for the $^5D_0 \rightarrow {}^7F_1$transition is also evident at 591 nm. Both electric– and magnetic–dipole transitions are evident even though luminescence intensities vary [39]. We could not find peak at 580 nm derived from the $^5D_0 \rightarrow {}^7F_0$ transition indicates that Eu^{3+} ions are in an asymmetric coordination environment which is corresponding with our previous inference of the coordination structure[40]. PNL-Tb2:1 has obvious green narrow-width emission. The emission bands were generated from the transitions between different energy levels of Tb^{3+} and were attributed to the $^5D_4 \rightarrow {}^7F_6$ (487 nm), $^5D_4 \rightarrow {}^7F_5$ (545 nm), $^5D_4 \rightarrow {}^7F_4$ (581 nm), and $^5D_4 \rightarrow {}^7F_3$ (620 nm) transitions. The weak PNL–Dy2:1 emission line assigned to the $^4F_{9/2} \rightarrow {}^6F_{13/2}$ (578 nm) transition and $^4F_{9/2} \rightarrow {}^6F_{15/2}$ (484 nm) transition was hardly observed. A broad peak at 350 nm to approximately 450 nm is

derived from the host matrix (PNL) which indicated that this kind of polysiloxane could not be made to luminescent material with dysprosium.

The carbonyl group can sensitize lanthanide emission, which is known as the "antenna effect" [41]. The energy absorbed by the organic group is transferred to the lanthanide ion. However, the sensitize degree varies for the difference of organic groups and lanthanide ions. As shown in Figure 5, the emission of the organic group consequently transformed into the characteristic emission of Eu^{3+} and Tb^{3+}. However, Dy^{3+} was not well sensitized. The fantastic luminescent property of Eu^{3+} and Tb^{3+} complexes also indicate the fine coordination between the lanthanide ions and the carbonyl group.

Luminescent elastomers were obtained after crosslinking process. We directly stimulate the elastomers at 298 K at a wavelength of 320 nm to discuss the luminescent properties of the elastomers. Emission spectra of the luminescent elastomer (PNL–Tb2:1–SH, PNL–Eu2:1–SH and PNL–Dy2:1–SH) are shown in Figure 6.

The characteristic emissions of Ln^{3+} did not change. The baselines of both PNL–Tb2:1–SH and PNL–Eu2:1–SH are fairly steady, and the broad peaks derived from the host matrix are hardly to observe; thus, the novel crosslinking network does not reduce the luminescence of lanthanide ion by inducing "fluorescence quenching". What is more, the remove of small molecules that may enhance the luminescence after crosslinking step endow the materials outstanding luminescent property. Both PNL–Tb2:1–SH and PNL–Eu2:1–SH showed quite narrow half peak width. Human eyes are sensitive to the monochromatic spectral lights of wavelengths *ca* 700 nm (red), 546 nm (green), and 436 nm (blue) according to the CIE1931 RGB colorimetric system. Therefore, the bright emissions of lanthanide

complexes in solids (silicone elastomers) can be easily observed by the naked eye upon illumination with 365 nm excitation light provided by a 100 w ultraviolet lamp, as shown in Fig. 1.

PL has been measured under different excitation wavelengths to use the PNL–Lns–SH as a tunable luminescent device. As shown in Fig .7, the highest PL intensity value at 617 nm was observed when λ_{exc} = 320 nm in PNL–Eu2:1–SH, whereas the lowest value was observed when λ_{exc} = 380 nm, thus showing that luminescence intensity is strongly dependent on excitation radiation. A muted output can be obtained by considering the PL band at 591 nm. The condition of PNL–Tb2:1–SH is similar to that of PNL–Eu2:1–SH. The highest PL value was measured at 547 nm when λ_{exc} = 320 nm, whereas the lowest was obtained at 360 nm. Luminescence intensity can shift between different low and high intensity values by changing the excitation wavelength [42].

Figure 5

Figure 6

Figure 7

Thermal properties of Ln^{3+} doped silicone elastomers

The thermal stability of complexes is very important because decomposition degrades the device performance of lanthanide ion complexes. TGA was conducted at a heating rate of 10 °C min^{-1} under a nitrogen atmosphere. Fig. 8 presents the thermogravimetric weight–loss curves of all complexes. All of the samples display similar weight–loss trends, as shown in the TGA curves of the PNLS elastomers. However, coordination with lanthanide ions altered the initial thermal decomposition temperature (T_d). T_d in PNL–Eu3:1–SH and

PNL–Eu2:1–SH decreased because of the chemical conjugated water in $Eu(NO_3)_3 \cdot 6H_2O$ [43]. The TG curves showed that the thermal decomposition temperatures of these two complexes were higher than 220 °C; thus, device fabrication by vacuum evaporation is feasible. Material decomposition occurred when temperature increased from 230 °C to 800 °C, and two distinct weight–loss regions were detected. PNL–SHs initially lost weight when temperature ranged from 230 °C to 465 °C because of organic decomposition. The mass losses of the organic components of PNL–Eu3:1–SH and PNL–Eu2:1–SH were 25.1 % and 35.2 %, respectively. Mass loss rate in the second weight–loss region from 465 °C to 800 °C slowed as a result of the decomposition of the heat–resistant Si–O and Si–C backbones [44].

Figure 8

Morphology of crosslinked silicone elastomers

SEM micrographs of the upper surface of the silicone elastomers are shown in Fig. 9. P1–SH (a) and PNL–SH (b) were obtained without lanthanide ion doping. Homogeneous surface morphologies were presented. Bonding NL to the silicone elastomer does not affect morphology. Phase separation did not occur in both PNL–Eu3:1–SH (c) and PNL–Eu2:1–SH (d) when lanthanide ions were incorporated into the matrices. The microscopic homogeneity of the elastomers can be observed with low inorganic lanthanide ion content. The lanthanide particles in silicone elastomer matrices are very well–dispersed, and did not aggregate. The phase interface between the lanthanide ion and the silicone matrix was not observed, thus indicating that the force between them was strong. Lanthanide particles intimately integrate into the elastomeric matrix [45].

Figure 9

DMA analysis

The modulus and dissipation factor (tan δ) of PNL–Eu3:1–SH and PNL–Eu2:1–SH, as a function of temperature are shown in Fig. 10, respectively. The α–transition peak height may be related to crosslinking density in amorphous polymers [46]. The glass–transition temperature of PNL–Eu3:1–SH is observed at –80 °C and tan δ is approximately 0.27, whereas those of PNL–Eu2:1–SH are –78 °C and 0.28. The peak values of tan δ of PNL–Eu–SHs decrease with the increase in Eu^{3+} content. Tan δ of the UV–cured elastomer shows a narrow glass–transition temperature range, which demonstrates the high uniformity of the formed thiol–ene network. This result proves that photo–polymerization occurs by the step–growth mechanism [47].

Figure 10

Contact angle measurement

Static contact–angle analysis was performed to study the effect of thiol–ene crosslinking on silicone elastomer hydrophilic performance. The image of the drop was calculated based on the shape of the drop (both left and right contact angles) with an accuracy of ± 0.1 ° using an image analysis system. Distilled water was used as the test liquid. All measurements were conducted at 25 °C. Silicone elastomer is typically a hydrophobic material with a water contact angle of approximately 109 ° ± 0.1 ° [48] . The contact angles of PNL elastomers were tested by a contact angle analyzer with distilled water (Fig. 11). P1–SH (a) was obtained directly from P1 and DBOET and does not contain an NL side chain. P1–SH has the largest contact angle at 105°, which was close to traditional silicone rubber. DBOET may decrease this angle slightly. Importing NAL as a side chain caused a sharp decrease in contact angle,

and this decrease is be attributed to hydrophilic –COOH, S, and other O atoms. The lanthanide ion–coordinated PNL has a lower contact angle than PNL and hydrophilia increases along with the increase in the proportion of lanthanide ion. Inorganic ion intake may increase the hydrophilia of the materials; thus, we can adjust the hydrophility of silicone elastomers by side–chain functionalization or inorganic ion doping. The novel luminescent elastomers obtained have lower contact angles compared with traditional silicone rubber. They can be applied in the aspects of oil resistance or sealing.

Figure 11

Solvent swelling and crosslinking density

We use the toluene swelling method to measure the crosslink density (v) and Mc of the obtained silicone elastomers. The results of solvent swelling and crosslinking density testing are listed in Table 3. The average molecular weight between the two junctions (Mc) is an important parameter in elastomer crosslinking. Mc decreases when v increases as a result of the physical and chemical actions of the polymer and the doped lanthanide ions. The crosslinking density increases with the increase in lanthanide ion ratio, and we suspect that the lanthanide ion acts as a crosslinker in the network when different chains are coordinated. The Mc of PNL–Eu3:1–SH is consistent with that of traditional heat–vulcanized silicone elastomers.

Table 3

4. Conclusion

A novel lanthanide ions-coordinated silicone elastomer has been successfully fabricated. This newly designed thiol–ene protocol can prepare polysiloxane–based luminescent products

under benign conditions compared with the traditional hydrosilylation method. P1 were partially functionalized by controlling the molar ratio of P1 and NAL. Residual vinyl groups can then be used as crosslinking sites to prepare luminescence elastomers. The novel crosslinked system does not affect the luminescent properties of the coordinated mixture. They show very intense photoluminescence under ultraviolet light and have very high coloric purity. The experimental results indicate complexing lanthanide ions reduced the contact angles. As a luminescent material, silicone elastomers may be applied in numerous fields in luminescent devices or in information technology. The combination of lanthanide ion and silicone elastomer, as well as the unique properties of these materials deserve further exploration.

Acknowledgments

This work was financially supported by the National Natural Science Foundation of China (No. 21274080 and 21204043), the Key Natural Science Foundation of Shandong Province of China (No.ZR2011BZ001).

References

1. S. Ida, C. Ogata, D. Shiga, K. Izawa, K. Ikeue and Y. Matsumoto, *Angew. Chem., Int. Ed.*, 2008, **47**, 2480-2483.
2. Y. Su, L. Li and G. Li, *Chem. Commun. (Camb.)*, 2008, 4004-4006.
3. R. Shunmugam and G. N. Tew, *Macromol. Rapid Commun.*, 2008, **29**, 1355-1362.
4. J.-C. G. Bünzli, *Acc. Chem. Res.*, 2006, **39**, 53-61.
5. R. J. Corriu and D. Leclercq, *Angew. Chem., Int. Ed. Engl.*, 1996, **35**, 1420-1436.
6. C. P. Hauser, D. T. Thielemann, M. Adlung, C. Wickleder, P. W. Roesky, C. K. Weiss

and K. Landfester, *Macromol. Chem. Phys*, 2011, **212**, 286-296.

7. X. F. Qiao and B. Yan, *J. Phys. Chem. B*, 2009, **113**, 11865-11875.

8. L.-H. Wang, W. Wang, W.-G. Zhang, E.-T. Kang and W. Huang, *Chem. Mater.*, 2000, **12**, 2212-2218.

9. Y. Cong, J. Fu, Z. Cheng, J. Li, Y. Han and J. Lin, *J. Polym. Sci., Part B: Polym. Phys*, 2005, **43**, 2181-2189.

10. W. Yin, M. Chen, T. Lu, M. Akashi and X. Huang, *Eur. Polym. J.*, 2006, **42**, 1305-1312.

11. Y. Okamoto, T. Kwei and D. Vyprachtický, *Macromolecules*, 1998, **31**, 9201-9205.

12. L.-M. Zhao and B. Yan, *J. Non-Cryst. Solids*, 2007, **353**, 4654-4659.

13. C. Y. Yang, V. Srdanov, M. R. Robinson, G. C. Bazan and A. J. Heeger, *Adv. Mater.*, 2002, **14**, 980-983.

14. L. D. Carlos, R. Sá Ferreira, J. Rainho and V. de Zea Bermudez, *Adv. Funct. Mater.*, 2002, **12**, 819-823.

15. L. N. Sun, H. J. Zhang, L. S. Fu, F. Y. Liu, Q. G. Meng, C. Y. Peng and J. B. Yu, *Adv. Funct. Mater.*, 2005, **15**, 1041-1048.

16. J. H. Harreld, A. Esaki and G. D. Stucky, *Chem. Mater.*, 2003, **15**, 3481-3489.

17. J. Pei, X.-L. Liu, W.-L. Yu, Y.-H. Lai, Y.-H. Niu and Y. Cao, *Macromolecules*, 2002, **35**, 7274-7280.

18. L. Liu, H. Lu, H. Wang, Y. Bei and S. Feng, *Appl. Organomet. Chem.*, 2009, **23**, 429-433.

19. F. Y. Zheng, J. Zhang and S. Y. Feng, *Rsc Advances*, 2013, **3**, 9957-9964.

20. Q. Lai, H. Lu, D. Wang, H. Wang, S. Feng and J. Zhang, *Macromol. Chem. Phys.*, 2011, **212**, 1435-1442.

21. H. Lu, L. Liu and S. Feng, *J. Appl. Polym. Sci.*, 2012, **123**, 1884-1888.

22. L. Liu, Y. L. Lu, L. He, W. Zhang, C. Yang, Y. D. Liu, L. Q. Zhang and R. G. Jin, *Adv. Funct. Mater.*, 2005, **15**, 309-314.

23. C. Barner- Kowollik, F. E. Du Prez, P. Espeel, C. J. Hawker, T. Junkers, H. Schlaad and W. Van Camp, *Angew. Chem., Int. Ed.*, 2011, **50**, 60-62.

24. C. E. Hoyle, T. Y. Lee and T. Roper, *J. Polym. Sci., Part A: Polym. Chem.*, 2004, **42**, 5301-5338.

25. J. W. Chan, C. E. Hoyle and A. B. Lowe, *J. Am. Chem. Soc.*, 2009, **131**, 5751-5753.

26. K. L. Killops, L. M. Campos and C. J. Hawker, *J. Am. Chem. Soc.*, 2008, **130**, 5062-5064.

27. M. I. Montanez, L. M. Campos, P. Antoni, Y. Hed, M. V. Walter, B. T. Krull, A. Khan, A. Hult, C. J. Hawker and M. Malkoch, *Macromolecules*, 2010, **43**, 6004-6013.

28. Y.-h. Li, D. Wang and J. M. Buriak, *Langmuir*, 2009, **26**, 1232-1238.

29. E. C. Hagberg, M. Malkoch, Y. Ling, C. J. Hawker and K. R. Carter, *Nano Lett.*, 2007, **7**, 233-237.

30. C. E. Hoyle and C. N. Bowman, *Angew. Chem., Int. Ed.*, 2010, **49**, 1540-1573.

31. L. Xue, D. X. Wang, Z. Z. Yang, Y. Liang, J. Zhang and S. Y. Feng, *Eur. Polym. J.*, 2013, **49**, 1050-1056.

32. R. Acosta Ortiz, A. Y. R. Martinez, A. E. García Valdez and M. L. Berlanga Duarte, *Carbohydr. Polym.*, 2010, **82**, 822-828.

33. S. Diao, K. Jin, Z. Yang, H. Lu, S. Feng and C. Zhang, *Mater. Chem. Phys.*, 2011, **129**, 202-208.

34. A.-C. Franville, D. Zambon, R. Mahiou and Y. Troin, *Chem. Mater.*, 2000, **12**, 428-435.

35. Z. Chen, Y. Wu, F. Huang, D. Gu and F. Gan, *Spectrochim. Acta, Part A*, 2007, **66**, 1024-1029.

36. F. Mercier, C. Alliot, L. Bion, N. Thromat and P. Toulhoat, *J. Electron Spectrosc. Relat. Phenom.*, 2006, **150**, 21-26.

37. J. Morales, J. Espinos, A. Caballero, A. Gonzalez-Elipe and J. A. Mejias, *J. Phys. Chem. B*, 2005, **109**, 7758-7765.

38. Y. Yue, Y. Liang, H. Wang, L. Feng, S. Feng and H. Lu, *Photochem. Photobiol.*, 2013, **89**, 5-13.

39. S. Fujihara and K. Tokumo, *Chem. Mater.*, 2005, **17**, 5587-5593.

40. A. F. Kirby and F. Richardson, *J. Phys. Chem.*, 1983, **87**, 2544-2556.

41. G. Crosby, R. Whan and R. Alire, *J. Chem. Phys.*, 1961, **34**, 743.

42. A. Gulino, F. Lupo, G. G. Condorelli, A. Motta and I. L. Fragalà, *J. Mater. Chem.*, 2009, **19**, 3507-3511.

43. Y.-Y. Li, B. Yan, L. Guo and Y.-J. Li, *Microporous Mesoporous Mater.*, 2012, **148**, 73-79.

44. W. Zhou, H. Yang, X. Guo and J. Lu, *Polym. Degrad. Stab.*, 2006, **91**, 1471-1475.

45. J. J. Han, H. F. Lu, J. Zhang and S. Y. Feng, *Mater. Chem. Phys.*, 2012, **136**, 36-42.

46. M. Di, S. He, R. Li and D. Yang, *Nucl. Instrum. Methods Phys. Res., Sect. B*, 2006,

248, 31-36.

47. J.-S. Kim, S. Yang, H. Park and B.-S. Bae, *Chem. Commun.*, 2011, **47**, 6051-6053.

48. J. T. Han, D. H. Lee, C. Y. Ryu and K. Cho, *J. Am. Chem. Soc.*, 2004, **126**, 4796-4797.

Captions for schemes, tables and figures

Scheme 1. Thiol–ene reaction mechanism.

Scheme 2. Synthesis of functionalized polysiloxanes (P1, P2, PNL, and T–PNL).

Scheme 3. Graphic of the crosslinking of the silicone elastomer networks.

Figure 1. Digital image of luminescent silicone elastomers under UV light (365 nm, 100 w). From left to right: PNL–Eu2:1–SH, PNL–Dy2:1–SH, and PNL–Tb2:1–SH.

Figure 2. Infrared spectra of [P1 , NAL, PNL, and PNL–Tb (a)], and [T–PNL and T–PNL–Eu (b)].

Figure 3. UV spectra of PNL (a) and T–PNL (b).

Figure 4. XPS of Tb 4d spectral regions in PNL–Tb and $Tb(NO_3)_3$.

Figure 5. Emission spectra of PNL–Tb2:1 (a), PNL–Dy2:1 (b) and PNL–Eu2:1 (c) before crosslinking in THF solution.

Figure 6. Emission spectra of PNL–Tb2:1–SH (a), PNL–Dy2:1–SH (b) and PNL–Eu2:1–SH (c) after crosslinking in silicone elastomer condition.

Figure 7. Emission spectra of PNL–Tb2:1–SH (a) and PNL–Eu2:1–SH (b) under different excitation wavelengths.

Figure 8. TGA of PNL–SH, PNL–Eu3:1–SH, and PNL–Eu2:1–SH.

Figure 9. SEM micrographs of P1–SH (a), PNL–SH (b), PNL–Eu3:1–SH (c), and PNL–Eu2:1–SH (d).

Figure 10. DMA curves of PNL–Eu3:1–SH and PNL–Eu2:1–SH. Modulus versus temperature [(a) and (c)] and Tan δ versus temperature [(b) and (d)].

Figure 11. Contact angles of the crosslinked elastomers P1–SH (a), PNL–SH (b),

PNLS–Eu3:1–SH (c), and PNL–Eu2:1–SH (d).

Table 1. GPC data on the obtained polymers.

Table 2. Various ratios of PNL–Ln–SHs (Ln = Eu, Tb, and Dy) complexes.

Table 3. Crosslink densities and Mc of elastomers when swollen at equilibrium.

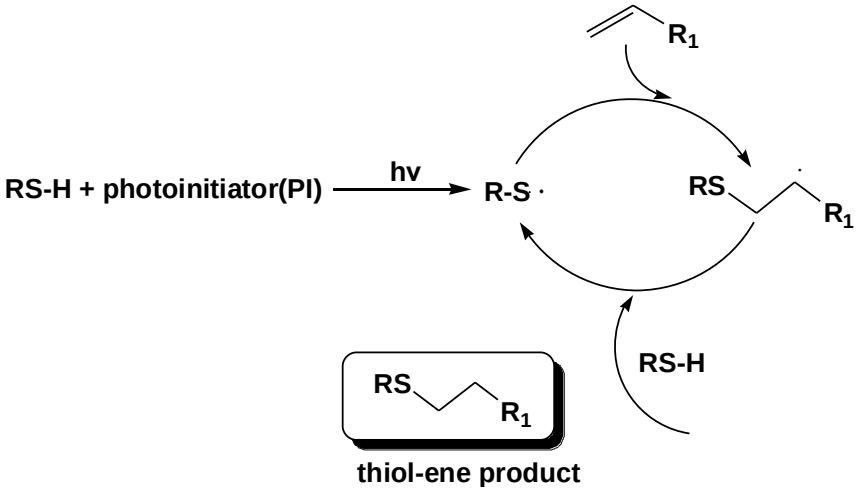

Scheme 1. Thiol–ene reaction mechanism.

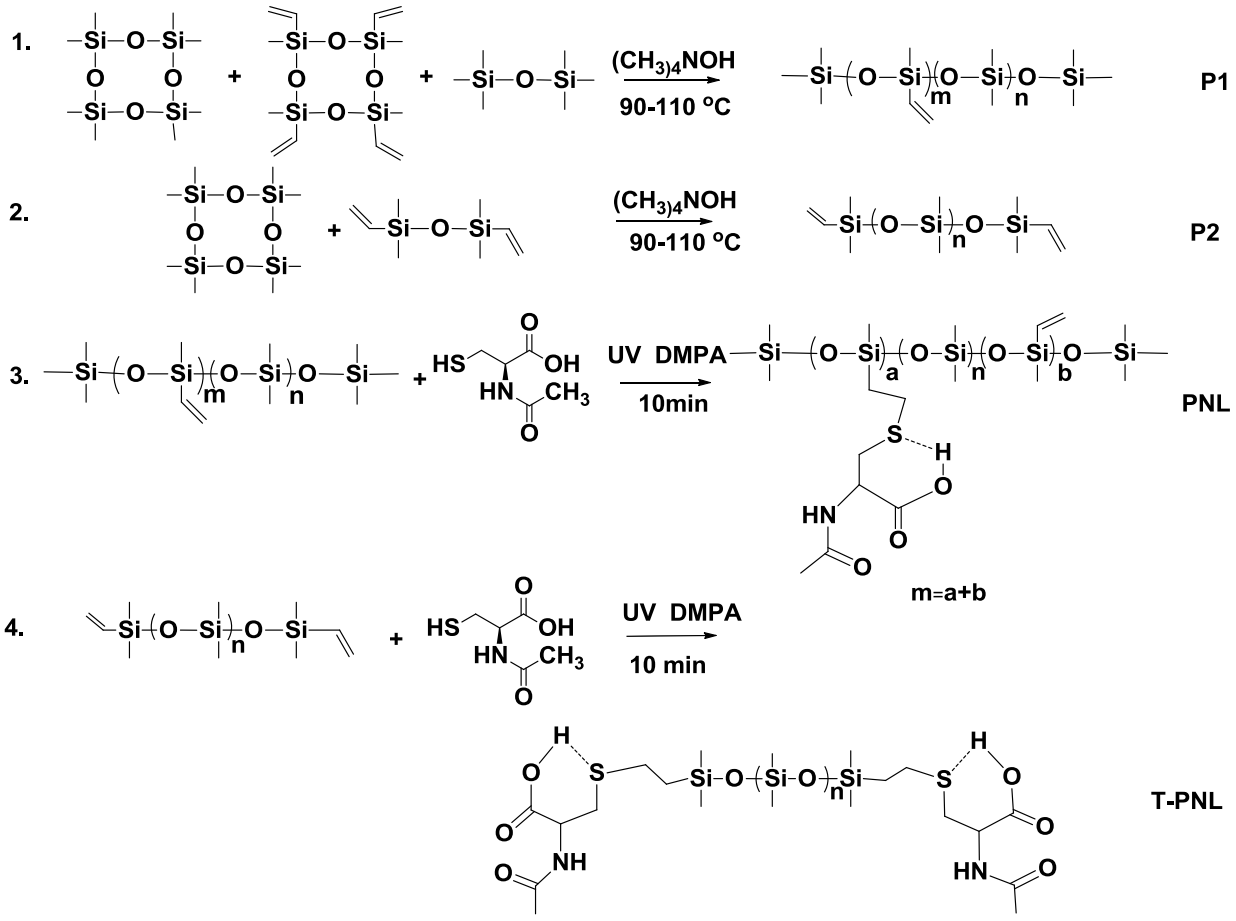

Scheme 2. Synthesis of functionalized polysiloxanes (P1, P2, PNL, and T–PNL).

The crosslinking step via thiol ene reaction:

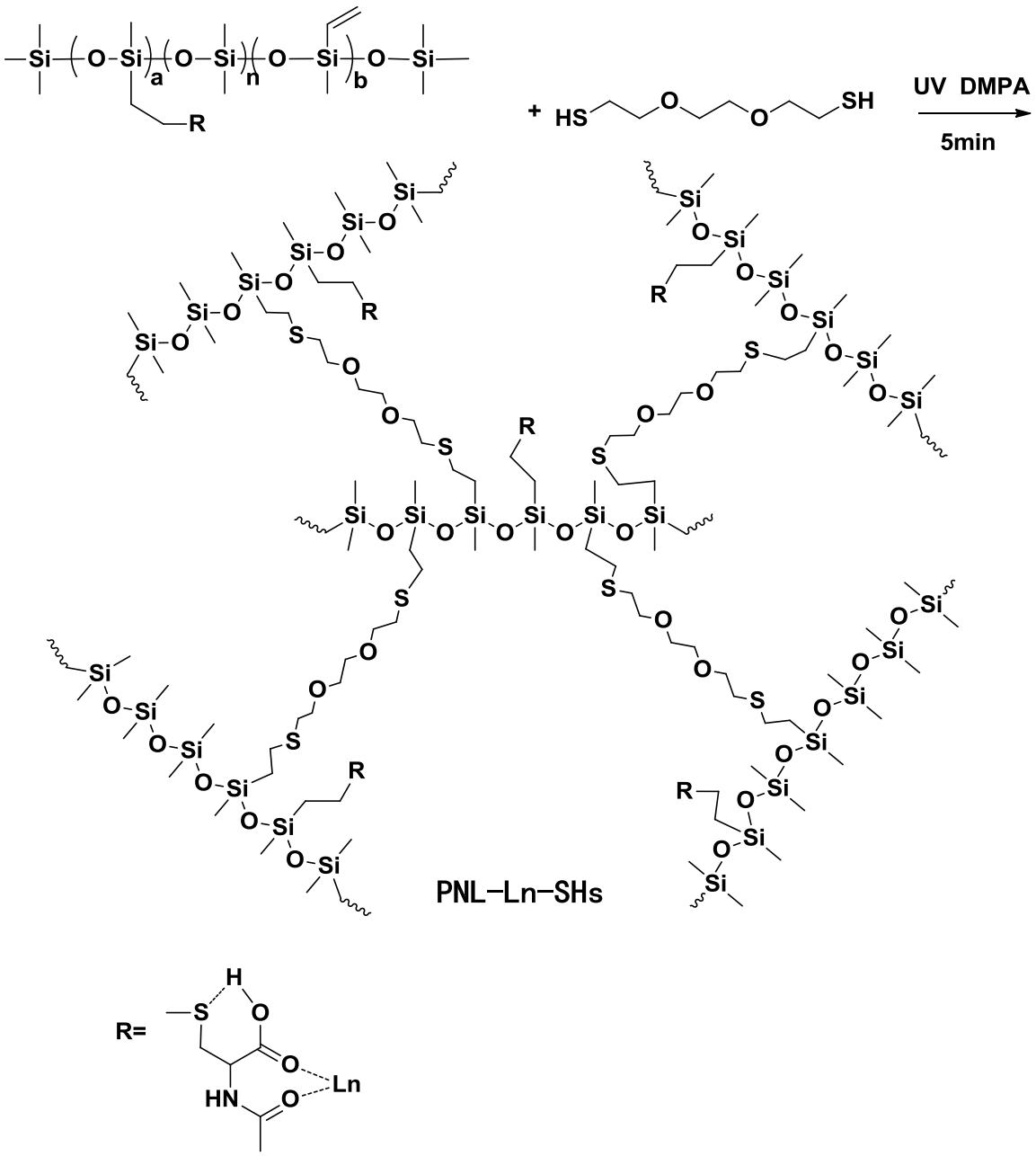

Scheme 3. Graphic of the crosslinking of the silicone elastomer networks.

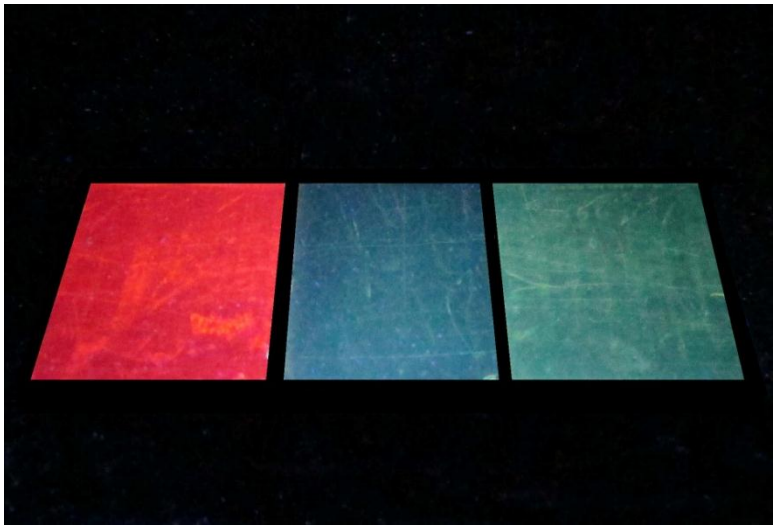

Figure 1. Digital image of luminescent silicone elastomers under UV light (365 nm, 100 w).

From left to right: PNL–Eu2:1–SH, PNL–Dy2:1–SH, and PNL–Tb2:1–SH.

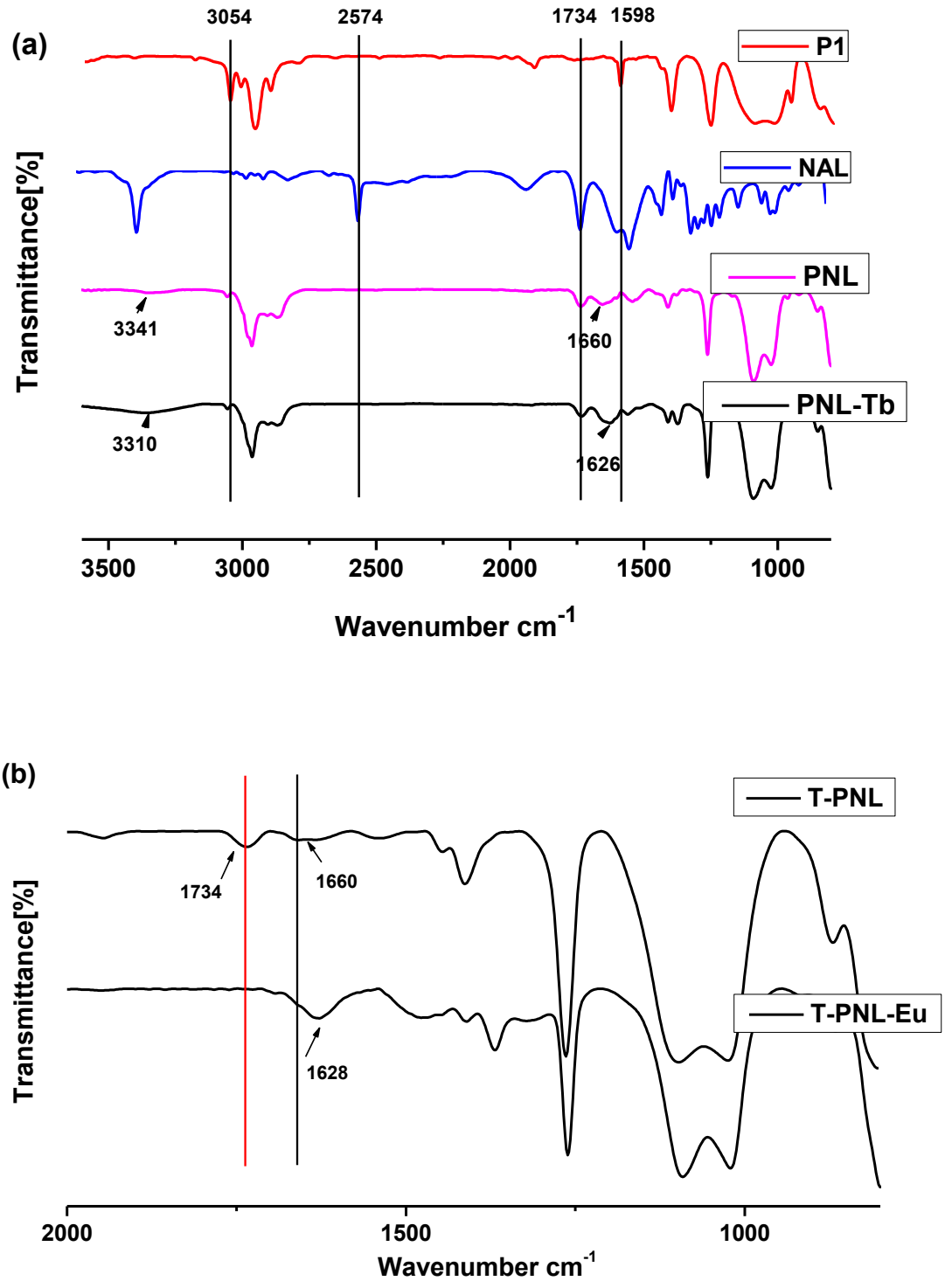

Figure 2. Infrared spectra of [P1 , NAL, PNL, and PNL–Tb (a)], and [T–PNL and T–PNL–Eu (b)].

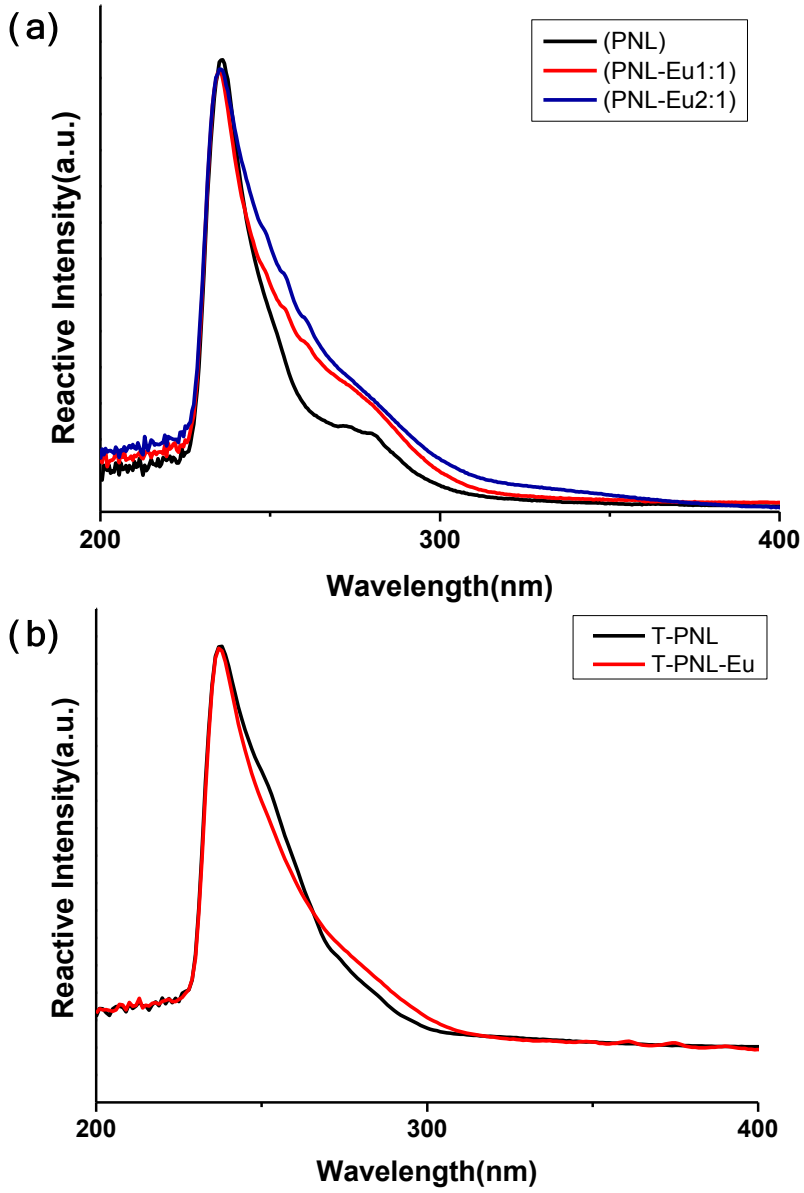

Figure 3. UV spectra of PNL (a) and T–PNL (b).

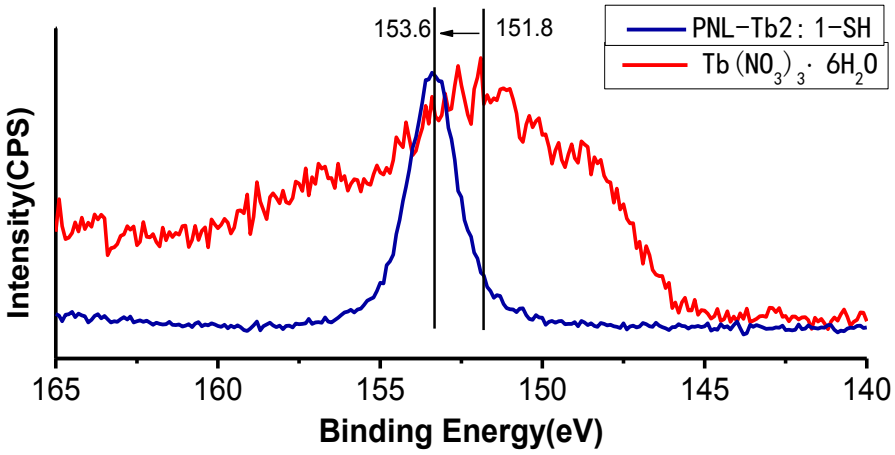

Figure 4. XPS of Tb 4d spectral regions in PNL–Tb and $Tb(NO_3)_3$.

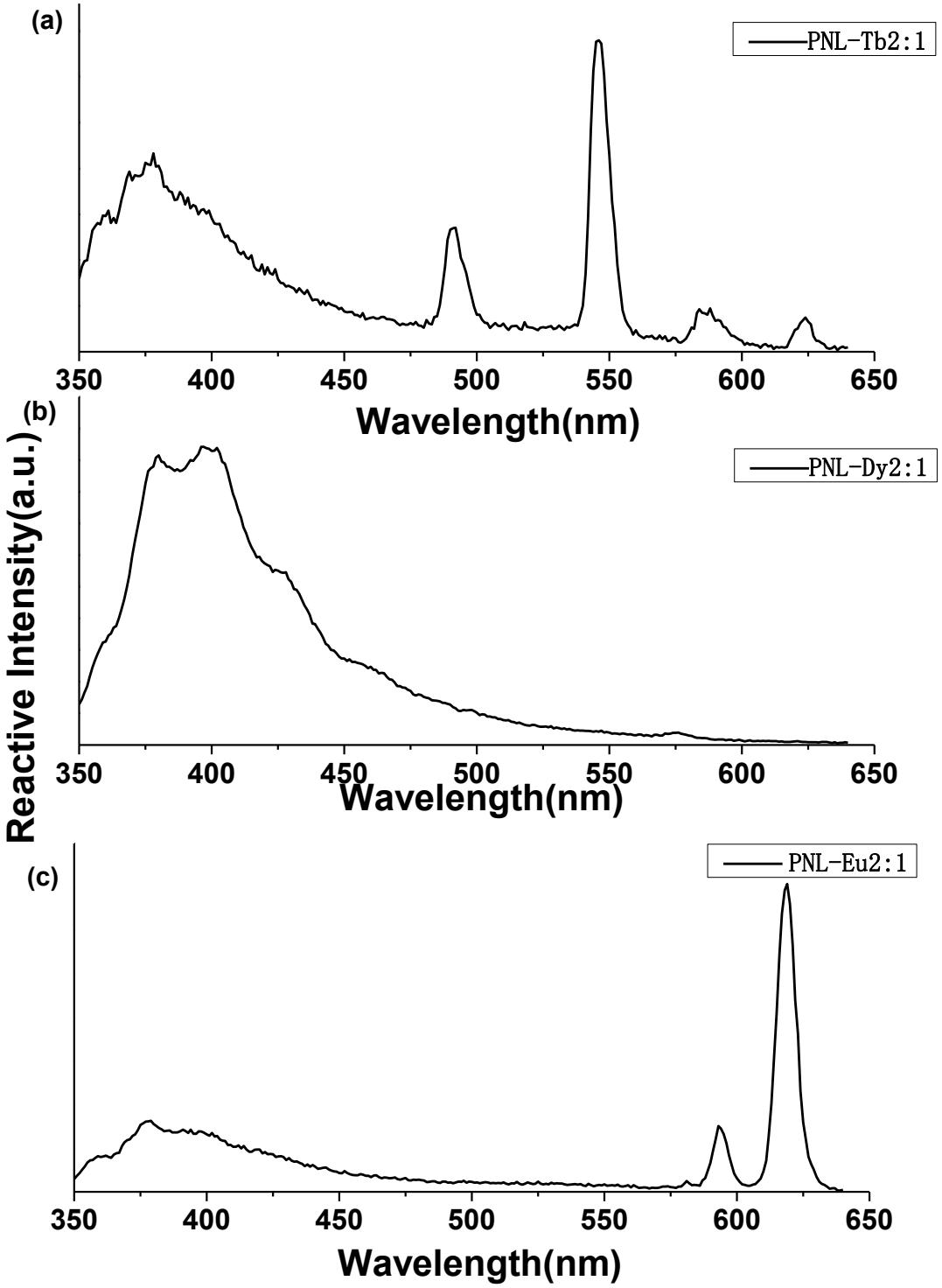

Figure 5. Emission spectra of PNL–Tb2:1 (a), PNL–Dy2:1 (b) and PNL–Eu2:1 (c) before crosslinking in THF solution

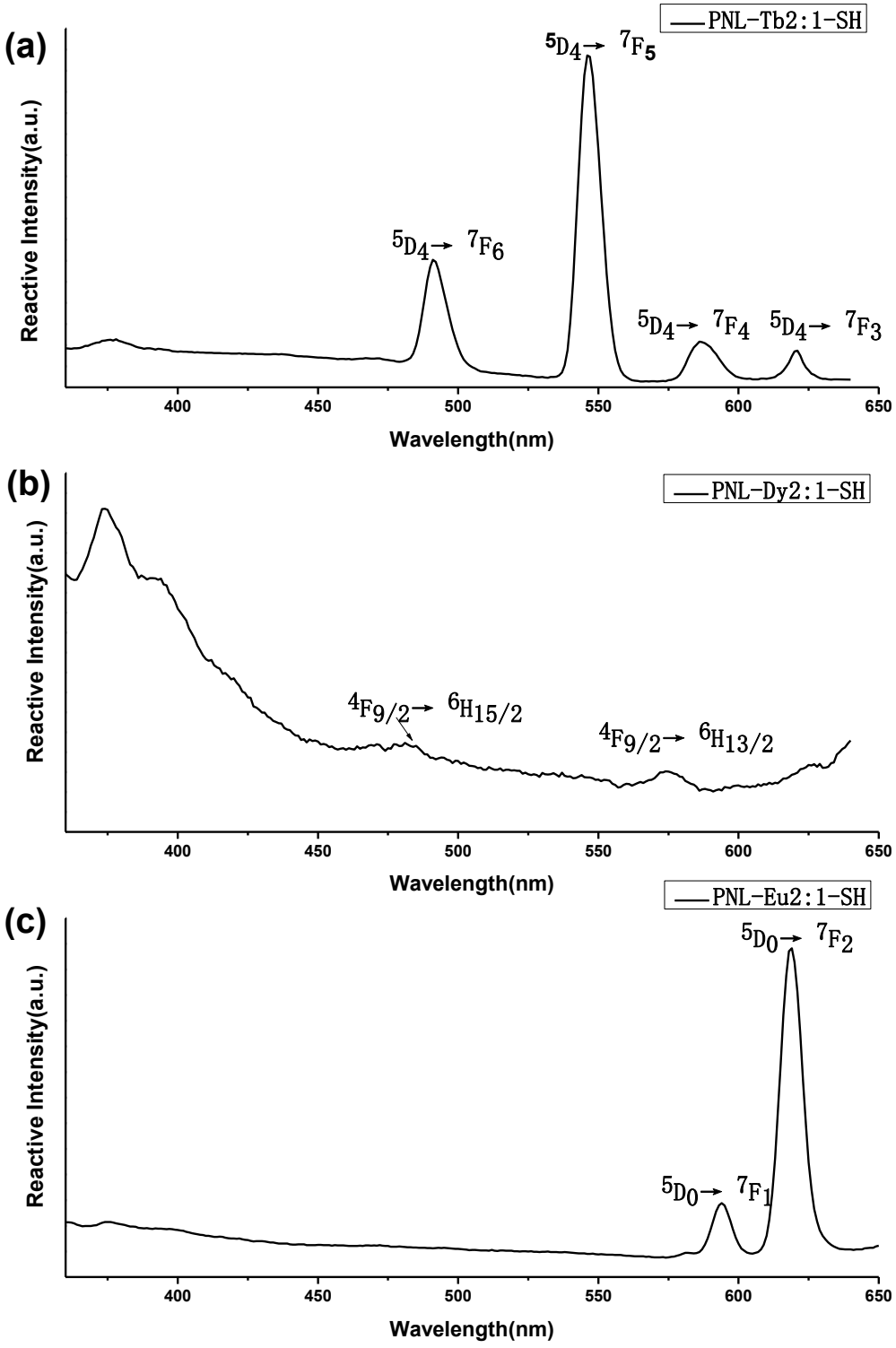

Figure 6. Emission spectra of PNL–Tb2:1–SH (a), PNL–Dy2:1–SH (b) and PNL–Eu 2:1–SH(c) after crosslinking in silicone elastomer condition.

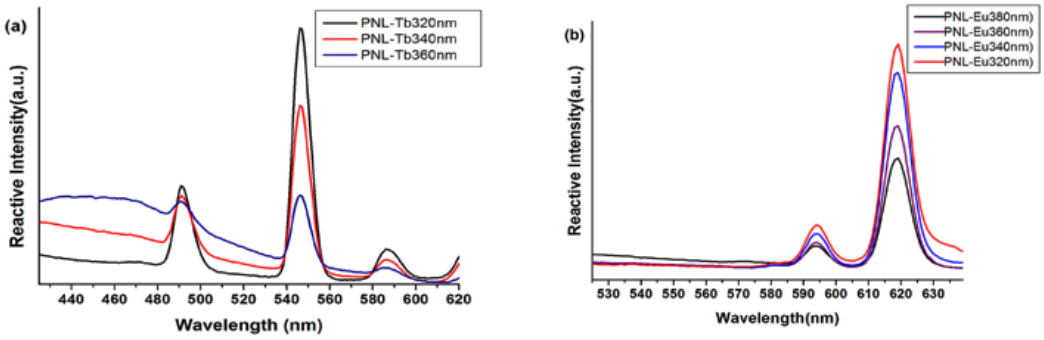

Figure 7. Emission spectra of PNL–Tb2:1–SH (a) and PNL–Eu2:1–SH (b) under different excitation wavelengths.

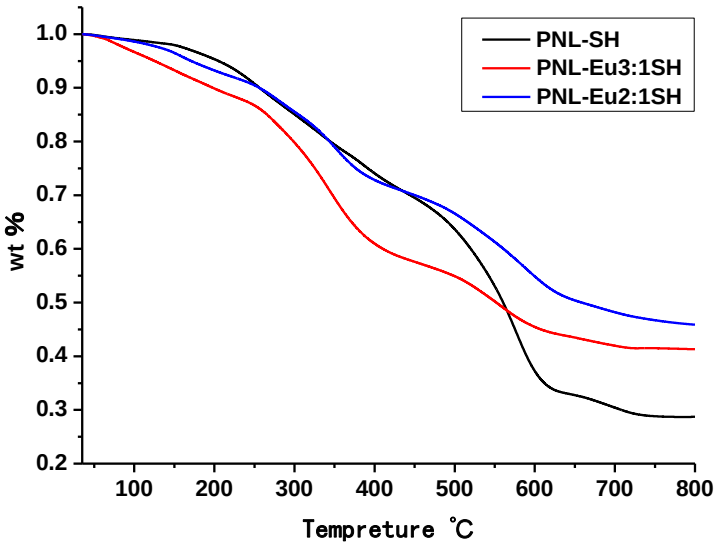

Figure 8. TGA of PNL–SH, PNL–Eu3:1–SH, and PNL–Eu2:1–SH.

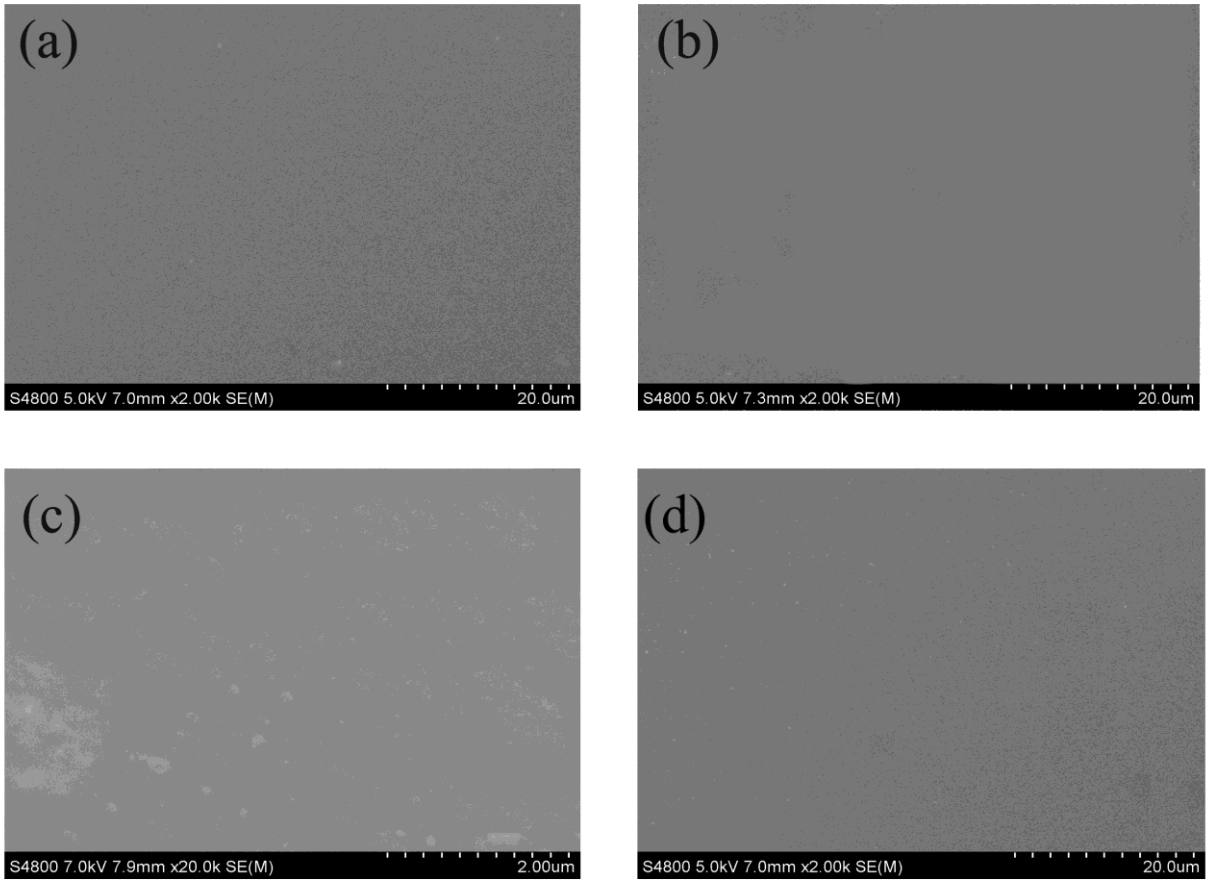

Figure 9. SEM micrographs of P1–SH (a), PNL–SH (b), PNL–Eu3:1–SH (c), and PNL–Eu2:1–SH (d).

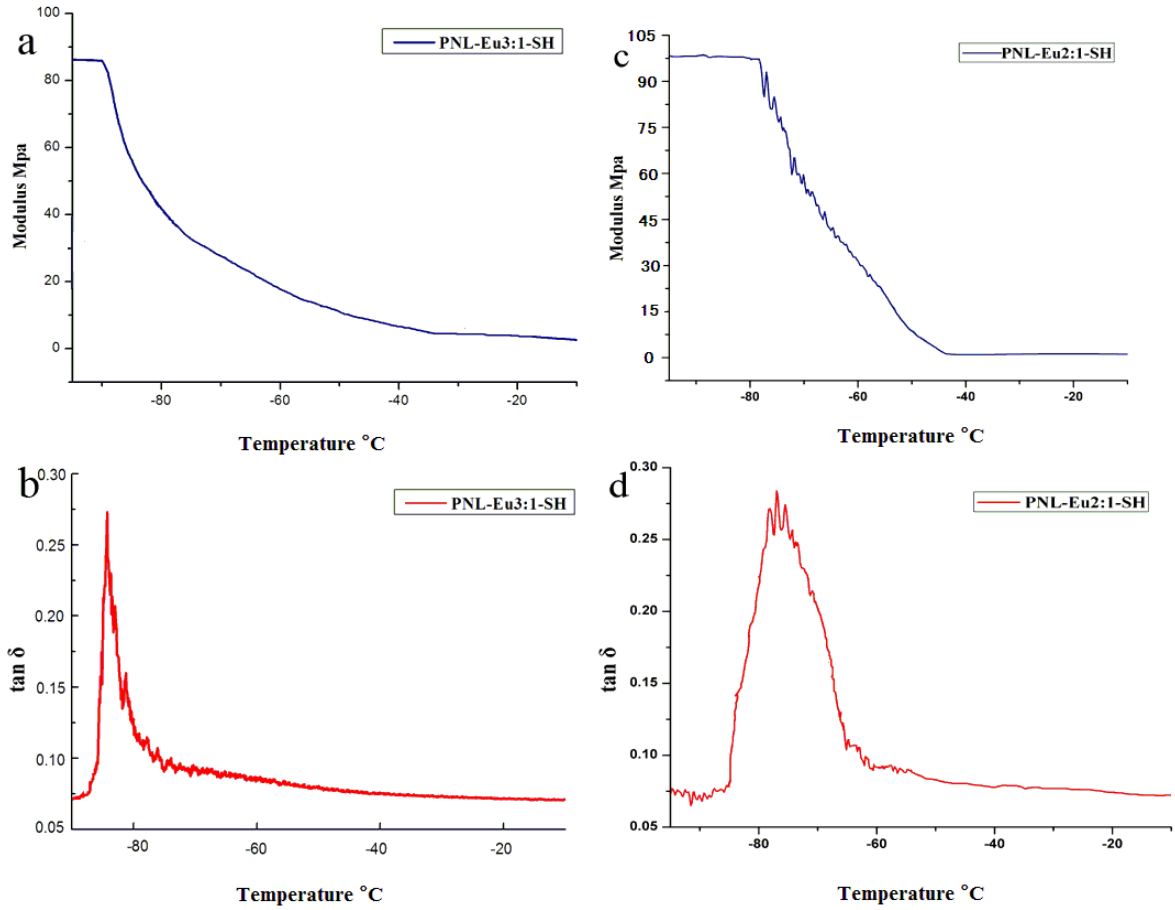

Figure 10. DMA curves of PNL–Eu3:1–SH and PNL–Eu2:1–SH. Modulus versus temperature [(a) and (c)] and Tan δ versus temperature [(b) and (d)].

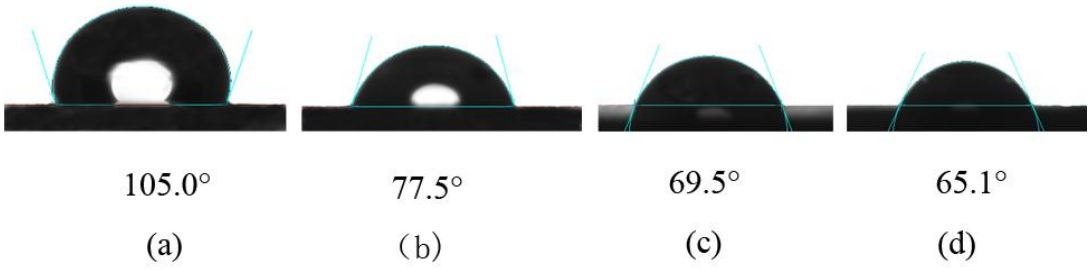

Figure 11. Contact angles of the crosslinked elastomers P1–SH (a), PNL–SH (b), PNLS–Eu3:1–SH (c), and PNL–Eu2:1–SH (d).

Table 1. GPC data on the obtained polymers.

Sample name	Mn (g/mol)	Mw (g/mol)	Mz (g/mol)	PDI	Mz/Mw
P1	62458	79650	102130	1.27	1.28
P2	10035	13421	17632	1.33	1.31
PNL	65039	83698	125645	1.28	1.50
T–PNL	10110	12680	17752	1.26	1.40

Table 2. Various ratios of PNL–Ln–SHs (Ln = Eu, Tb, and Dy) complexes.

Sample name	Molar ratios C=O: Ln^{3+}	PNL or T–PNL (g)	$Ln(NO_3)_3 \cdot 6H_2O$ (g)	DBOET （g）
PNL–Eu1:1	2:1	5.08	2.33	–
PNL–Eu2:1	4:1	2.54	0.58	–
PNL–Tb2:1	4:1	2.54	0.59	–
PNL–Dy2:1	4:1	2.54	0.60	–
PNL–Eu2:1–SH	4:1	5.08	1.16	0.02
PNL–Eu3:1–SH	6:1	5.08	0.77	0.02
PNL–Tb2:1–SH	4:1	5.08	1.18	0.02
PNL–Dy2:1–SH	4:1	5.08	1.19	0.02
T–PNL–Eu	4:1	1.00	0.02	–

Table 3. **Crosslink densities and Mc of elastomers when swollen at equilibrium**.

Sample name	Swelling (%)	φ	Crosslinking density ve×10^4（mol/cm^3）	Mc (g/mol)
P1–SH	295	0.18	1.22	7051
PNL–SH	184	0.31	1.75	4927
PNL–Eu3:1–SH	155	0.37	2.64	3270
PNL–Eu2:1–SH	112	0.40	3.63	2521